Progress In Electromagnetics Research, Vol. 123, 467–484, 2012

A NOVEL ESTIMATION APPROACH OF DYNAMIC AND COUPLING BASELINE FOR DISTRIBUTED SATELLITE SAR

L. Feng*, H. P. Xu, C. S. Li, S. Li, and H. Gao

School of Electronic and Information Engineering, Beihang University, Beijing, China

Abstract—In distributed satellite synthetic aperture radar (DS-SAR), along-track and cross-track baselines couple with each other and change dynamically due to formation flying, which makes it difficult to estimate interferometric baseline accurately. To solve the problem, a novel high-precision baseline estimation approach based on interferometric phase is proposed. By modeling accurate relationship between coupling baselines and two-dimensional (azimuth and range) inteferometric fringe frequency under the ellipsoid earth model, the along-track and cross-track baseline can be estimated separately by interferometric phase decoupling. By selecting several segments from interferometric phase during the whole data-take time and estimating instantaneous baseline of each segment, the dynamic baseline can be obtained via a linear filtering. Besides, to improve the baseline estimation accuracy, Semi-Newton iterative method is applied to acquire high-precision fringe frequency estimation, which can make the baseline estimation achieve centimeter level precision. The simulation validates the approach.

1. INTRODUCTION

Distributed satellite synthetic aperture radar (DS-SAR) is a new earth observation system, in which several satellites work cooperatively. The system has three major applications: high-resolution wide-swath imaging, producing global high-precision digital elevation model (DEM) data and ground moving target indication (GMTI) [1, 2].

Baseline determines performance of interferometric SAR (InSAR) system and is also an important parameter in elevation reversion.

Received 31 August 2011, Accepted 15 November 2011, Scheduled 6 January 2012

* Corresponding author: Liang Feng (fengliang0419@sina.com).

Therefore, baseline estimation is very important in data processing of InSAR system [3–5].

For conventional spaceborne InSAR system, baseline can be estimated from satellite state vector [6], interferometry calibration (using Ground Control Points (GCPs) [7–9], coarse DEM data [10] or sea surface data [11]) or interferometric phase information [12, 13]. The precision of satellite state vector method is usually low due to its dependence on satellite positioning. In the method based on GCPs, known altitude and interferometric phase are used to calculate the baseline parameters based on geometry relationship in InSAR system. But it needs high precise layout and measurement of GCPs [14–16], which is hard to fulfill. The method based on DEM cannot obtain precise estimation due to the poor quality of reference DEM data. The calibration method based on sea surface is proposed in literature [11] for spaceborne single-pass dual-antenna interferometry without along-track baseline. The correlation of signals from different SAR antennas is low due to movement of sea surface. The estimation metod based on interferometric phase information [12] uses typical two-dimensional (2-D) geometry of InSAR to deduce the relationship between interferometric fringe frequency and cross-track baseline, without considering curvature of the earth. The method is used widely, because there is no need for satellite orbit ephemerides or accurate information of GCPs.

Satellites in DS-SAR system formate according to specific rules, so that baselines can be configured expediently [2], which are usually coupled for formation flying [17], that is, along-track baseline and cross-track baseline exist simultaneously [18, 19]. The coupling baselines induces coupling problem in the interferometric phase [4]. Furthermore, the baseline is three-dimensional (3-D) and also changes dynamically during the data-take time due to formation flying of satellites in the system [19]. Therefore, it is hard to obtain high precise DS-SAR baseline data.

Xu separates along-track baseline and cross-track baseline through image registration, and estimates the two kinds of baseline errors by image registration and subspace decomposition respectively [20]. However, the method requires very high precision of image registration. Another method [21] is to measure the relative state vector between satellites based on differential Global Positioning System (DGPS), laser and radio. But in DS-SAR, measured baseline is different from interferometric baseline. It may introduce errors when converting the measured baseline.

The precision of baseline estimation method, based on interferometric phase information in literature [12], is low because of unac-

curate geometry relationship and low-precision fringe frequency estimated through Fourier analysis. A novel method to achieve DS-SAR baseline estimation based on interferometric phase information is proposed in this paper. The method makes improvements from five aspects. Firstly, accurate 3-D geometry relationship is set up for high resolution DS-SAR system. Secondly, a new method to decompose coupling interferometric phase into two parts related to along-track baseline and cross-track baseline respectively is proposed as well. Thirdly, accurate mathematical relationship between the coupling baseline and the 2-D interferometric fringe frequency is deduced under the ellipsoid earth model. Fourthly, several segments of interferometric phase data are selected to acquire the dynamic variation model of the baseline via a linear filtering process with estimated instantaneous baselines. Furthermore, Semi-Newton iterative method is applied to estimate high-precision fringe frequency to improve baseline estimation precision.

This paper is structured as follows. Section 2 investigates the mathematical model of DS-SAR interferometric phase and decomposition of the coupling interferometric phase. In Section 3, theory of coupling baseline estimation is presented. Section 4 depicts the framework and implementation method of baseline estimation, while emphatically explaining fringe frequency estimation method based on Semi-Newton method. In Section 5, simulation validates the high-precision baseline estimation method. Conclusion is given in the final section.

2. MATHEMATIC MODEL OF INTERFEROMETRIC PHASE FOR DS-SAR

To present interferometric signal model, the spatial geometry of two satellites formation DS-SAR is shown in Fig. 1. A 3-D coordinate system is adopted. The system is fixed to centroid of the master satellite, where Z-direction is along the line between the earth and the master satellite, positive earth deviation. The X-direction is the master satellite velocity direction, and Y-direction is orthogonal in the right hand system to X.

S_m and S_s denote the master and slave satellite, respectively. Radar signals are transmitted from SAR antenna on the master satellite, while being received by both the master satellite SAR antenna and the slave satellite SAR antenna. S'_s is the projection of S_s in the YZ plane. V_m represents the velocity of master satellite and V_s represents the velocity of slave satellite. Here, V_m and V_s are parallel to the X axis. H_m is the height of the master satellite. N denotes the nadir of the master satellite. O is the geo-center and R_e denotes

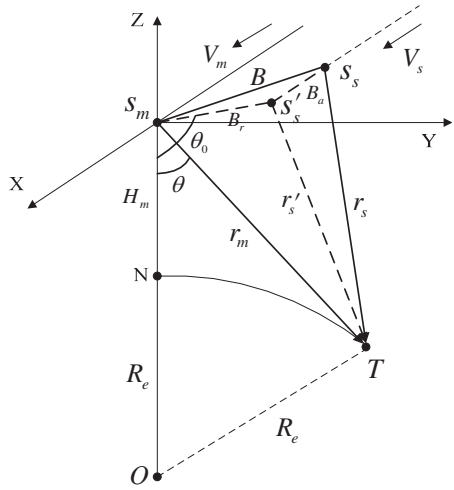

Figure 1. Spatial geometry model of DS-SAR.

the local earth radius. B is the baseline, which can be expressed as the vector (B_a, B_y, B_z) in the 3-D coordinate system. B_a is along-track baseline, B_y is the horizontal component of cross-track baseline B_r and B_z is the vertical component. Here,

$$B_y = B_r \cdot \sin\theta_0 \tag{1}$$

$$B_z = -B_r \cdot \cos\theta_0 \tag{2}$$

θ_0 is the angle between cross-track baseline B_r and the negative Z-direction. θ represents the look angle of master satellite SAR. r_m is the slant range between the phase center of master satellite SAR antenna and the ground target T, and r_s is the slant range between the phase center of slave satellite SAR antenna and T. r_s' is the projection of r_s in the YZ plane.

The single look complex (SLC) SAR data pair can be obtained through range pulse compression and azimuth processing [22] on echoes from the master and slave satellite SAR. The model can be expressed as [22, 23]:

$$\begin{aligned} s_m(r,x) &= \sigma(r,x) \otimes \exp\left\{-j\frac{4\pi}{\lambda}r_m\right\} \cdot \exp\left\{-j2\pi f_{dm} \cdot \frac{x}{V}\right\} \\ &\quad \otimes [w_r(r)\, w_a(x)] + n_m \end{aligned} \tag{3}$$

$$\begin{aligned} s_s(r,x) &= \sigma(r,x) \otimes \exp\left\{-j\frac{2\pi}{\lambda}(r_m + r_s)\right\} \cdot \exp\left\{-j\pi\left(f_{dm} + f_{ds}'\right) \cdot \frac{x}{V}\right\} \\ &\quad \otimes [w_r(r)\, w_a(x)] + n_s \end{aligned} \tag{4}$$

where $\sigma(r,x)$ is the backscatter coefficient, r and x respectively are coordinates in the slant range direction and azimuth direction. $w_r(r)$ and $w_a(x)$ respectively represent the impulse response functions of point target in range and azimuth direction. n_m and n_s denote the systematic thermal noises. f_{dm} and f_{rm} respectively are the Doppler centroid frequency and modulation frequency of master satellite, while f'_{ds} and f'_{rs} represent that of salve satellite under assumption that it is in the transmitting and receiving model. Here, the slave SAR is in the receiving-only model, so that the overall contribution of Doppler of slave satellite is [24].

$$\begin{cases} f_{ds} = (f_{dm} + f'_{ds})/2 \\ f_{rs} = (f_{rm} + f'_{rs})/2 \end{cases} \tag{5}$$

Through formula (3) and (4), the interferometric phase can be given as following:

$$\phi = \arg\left(s_m(r,x) \cdot s_s^*(r,x)\right) = \frac{2\pi}{\lambda}(r_s - r_m) + \pi\left(f'_{ds} - f_{dm}\right)\frac{x}{V} \tag{6}$$

In Equation (6), the first term is related to slant range, and the second to doppler information. The first phase component is mainly introduced by cross-track baseline information, denoted as ϕ_r, namely:

$$\phi_r = \frac{2\pi}{\lambda}(r_s - r_m) \tag{7}$$

The second phase component of formula (6) is introduced by along-track baseline information denoted as ϕ_a, namely:

$$\phi_a = \pi\left(f'_{ds} - f_{dm}\right)\frac{x}{V} = 2\pi\left(f_{ds} - f_{dm}\right)\frac{x}{V} \tag{8}$$

3. COUPLING BASELINE ESTIMATION THEORY BASED ON INTERFEROMETRIC FRINGE FREQUENCY

This section deduces the relationship between coupling baseline and 2-D interferometric fringe frequency in DS-SAR.

3.1. Instantaneous along-track Baseline Estimation

Along-track baseline in DS-SAR causes different squint angles of master satellite and slave satellite, which leads to different Doppler centroid frequencies. Therefore, the along-track baseline can be calculated via the difference of Doppler centroid frequencies.

Along-track geometry of DS-SAR is given in Fig. 2, where φ_m and φ_s are squint angles of master satellite and slave satellite, respectively.

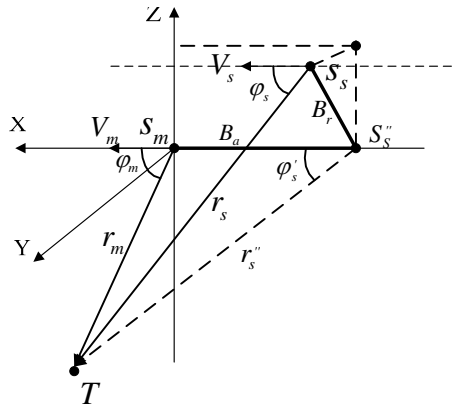

Figure 2. Along-track geometry of DS-SAR.

S_S'' is the projection of S_s on the X axis, B_a is the along-track baseline, r_s'' is the slant range between S_S'' and the target T and φ_s' is the angle from r_s'' to the X axis. Based on the geometry, f_{dm} and f_{ds}, which represent Doppler centroid frequencies of master satellite and slave satellite, are obtained [25]:

$$f_{dm} = -\frac{2V}{\lambda}\cos\varphi_m \tag{9}$$

$$f_{ds} = -\frac{V}{\lambda}\left(\cos\varphi_m + \cos\varphi_s\right) \tag{10}$$

From Equations (9) and (10), the difference of Doppler centroid frequencies is calculated as:

$$\begin{aligned}\Delta f_d(m,s) = f_{ds} - f_{dm} &= \frac{V}{\lambda}\left(\cos\varphi_m - \cos\varphi_s\right) \\ &= \frac{2V}{\lambda}\sin\left(\frac{\varphi_s-\varphi_m}{2}\right)\sin\left(\frac{\varphi_m+\varphi_s}{2}\right) \approx \frac{VB_a\sin\varphi}{\lambda r_m}\end{aligned} \tag{11}$$

where we assume that

$$\varphi = \left(\varphi_m + \varphi_s\right)/2 \tag{12}$$

$$\varphi_s \approx \varphi_s', \quad (V_s//X\ axis, B_r \ll r_s) \tag{13}$$

$$\sin\left(\frac{\varphi_s-\varphi_m}{2}\right) \approx \frac{\varphi_s-\varphi_m}{2} \approx \frac{\varphi_s'-\varphi_m}{2} \approx \frac{B_a}{2r_m}, \ \left(\frac{\varphi_s-\varphi_m}{2} \ll \pi\right) \tag{14}$$

It is indicated from Equation (11) that the relationship between difference of Doppler centroid frequencies $\Delta f_d(m,s)$ and along-track baseline B_a is linear.

Based on Equation (8), we have:

$$\phi_a = 2\pi \left(f_{ds} - f_{dm}\right) \frac{x}{V} = 2\pi \cdot \Delta f_d \left(m, s\right) \cdot t_a \tag{15}$$

where $t_a = x/V$ represents azimuth time. It is indicated from Equation (15) that the relationship between the difference of Doppler centroid frequencies $\Delta f_d \left(m, s\right)$ and the azimuth component of interferometric phase ϕ_a is linear in short time as well. By analyzing ϕ_a, along-track baseline can be solved via Equation (16), as follows:

$$B_a \left(m, s\right) \approx \frac{\lambda r_m \Delta f_d \left(m, s\right)}{V \sin \varphi} \tag{16}$$

where $\Delta f_d \left(m, s\right)$ is obtained through interferometric fringe frequency estimation in azimuth direction. Then along-track baseline B_a can be estimated by Equation (16).

3.2. Instantaneous Cross-track Baseline Estimation

Based on geometry in Fig. 1, $\cos\theta$ can be denoted as a function $f\left(r_m\right)$ with regard to r_m [12]:

$$f\left(r_m\right) = \cos\theta \tag{17}$$

In flat terrain, frequency of range interferometric fringe is

$$k_{r_m} = \frac{d\phi_r}{dr_m} = -\frac{2\pi B_r}{\lambda} \cos\theta_0 \cdot f'(r_m) + \frac{2\pi B_r}{\lambda} \sin\theta_0 \frac{f\left(r_m\right) \cdot f'\left(r_m\right)}{\sqrt{1 - f^2\left(r_m\right)}} \tag{18}$$

The differential coefficient of k_{r_m} is

$$\begin{aligned} \frac{dk_{r_m}}{dr_m} &= -\frac{2\pi B_r}{\lambda} \cos\theta_0 \cdot f''\left(r_m\right) \\ &\quad + \frac{2\pi B_r}{\lambda} \sin\theta_0 \frac{\left[f'\left(r_m\right)\right]^2 + f\left(r_m\right) \cdot f''\left(r_m\right) \sin^2\theta}{\sin^3\theta} \end{aligned} \tag{19}$$

It can be proved that frequency of interferometric fringe k_{r_m} in flat terrain is varying with the slant range of master satellite r_m monotonously. Because in flat terrain,

$$\frac{dk_{r_m}}{dr_m} > 0 \tag{20}$$

As k_{r_m} is a function upon length and tilted angle of cross-track baseline from Equation (18), cross-track baseline can be acquired according to information on frequency of range interferometric fringe. Once instantaneous frequencies of range interferometric fringe corresponding to two slant range coordinates r_m's are estimated repectively, cross-track baseline B_r and tilted angle θ_0 can be solved.

Two functions $F(r_m)$ and $G(r_m)$ with regard to the slant range of master satellite are defined as:

$$\begin{cases} F(r_m) = \frac{2\pi}{\lambda} f'(r_m) \\ G(r_m) = \frac{f(r_m)}{\sqrt{1-f^2(r_m)}} \end{cases} \tag{21}$$

In which, $r_m^{\min}$ and $r_m^{\max}$ represent the nearest and farthest slant range of master satellite SAR data selected, $k_{r_m^{\min}}$ and $k_{r_m^{\max}}$ are the frequencies of interferometric fringe corresponding to $r_m^{\min}$ and $r_m^{\max}$. Equation as follows can be deduced from Equations (18) and (21):

$$\begin{bmatrix} F\left(r_m^{\min}\right) \cdot G\left(r_m^{\min}\right) & F\left(r_m^{\min}\right) \\ F\left(r_m^{\max}\right) \cdot G\left(r_m^{\max}\right) & F\left(r_m^{\max}\right) \end{bmatrix} \cdot \begin{bmatrix} B_y \\ B_z \end{bmatrix} = \begin{bmatrix} kr_m^{\min} \\ kr_m^{\max} \end{bmatrix} \tag{22}$$

Thus, the cross-track baseline can be obtained.

4. REALIZATION OF DS-SAR BASELINE ESTIMATION

Deducing the calculation formula of along-track and cross-track baseline, as Equations (16) and (22), the high-precision estimation method of dynamic coupling baseline is proposed in this section, with implementation steps provided as well.

Besides coupling problem, there is dynamic variation of DS-SAR baseline in along-track direction during the whole data-take time. Since it can be considered stable during short interval, several interferometric phase data segments can be selected with short interval in along-track direction. As long as there is no drastic topographic relief of each segment, instantaneous baseline of each segment can be estimated with high precision, and dynamic baseline variation rule in long time can be obtained via interpolation and fitting. This section focuses on the framework of dynamic baseline estimation and implementation in detail. Then, in order to improve the estimation accuracy of interferometric fringe frequency, which is an important technology in the baseline estimation, we introduce the Semi-Newton iterative method.

4.1. Implementation Steps for Dynamic and Coupling Baseline Estimation

Figure 3 shows the flowchart of dynamic and coupling baseline estimation of DS-SAR. The whole estimation process includes three main steps:

(1) Performing SLC Imaging [26–28] and interferomery, which can be implemented by three additional steps.

(a) Getting SLC SAR data pair using DS-SAR imaging algorithm.

(b) Achieving registration of both master and slave SAR images via coarse registration, interpolation and precise registration [29, 30].

(c) Generating interferometric phase data via interferometry and phase filtering [31].

(2) Selecting N segments of interferometric phase, which correspond to relatively flat terrain, to estimate the instantaneous baseline in both along-track and cross-track direction of each segment. As seen from Fig. 3 inside the blue pane, it can be performed by three additional steps.

(a) Obtaining the Doppler centroid frequency difference of master satellite and slave satellite $\Delta f_d(m,s)$ by interferometric fringe frequency estimation of ith data segment to calculate along-track baseline B_a via Equation (16).

(b) Acquiring the minimum and maximum value of frequencies $k_{r_m^{\min}}$ and $k_{r_m^{\max}}$, which correspond to the nearest and farthest slant range of the data segment, by estimating the interferometric fringe frequency in range direction. Then calculate the two components B_y and B_z of cross-track baseline with known $k_{r_m^{\min}}$, $k_{r_m^{\max}}$ and other parameters via Equations (18), (21)–(22).

(c) Obtaining instantaneous baseline vector $\mathbb{B}_i = (B_a, B_y, B_z)$, $i = 1, \ldots, N$ of the ith data segment.

(3) Concluding 3-D baseline variation rule with azimuth time $\mathbb{B}(t_a) = [B_a(t_a), B_y(t_a), B_z(t_a)]$, by interpolating and fitting N baseline vectors $\mathbb{B}_i$ $(i = 1, \ldots, N)$, where t_a denotes the azimuth time (in along-track direction).

4.2. Interferometric Fringe Frequency Estimation Based on Semi-Newton Iterative Method

The 2-D (azimuth and range direction) interferometric fringe frequency estimation method is proposed in this section. The estimation accuracy of traditional interferometric fringe frequency estimation method, based on Fourier transform, cannot satisfy the DS-SAR system perfectly. In order to improve estimation precision, Semi-Newton iterative method, applied in the implementation steps (2a) and (2b) shown in Fig. 3, is introduced to estimate fringe frequency.

It is assumed that there are N phase data segments selected in azimuth direction, denoted as $PhaseData_i (i = 1, \ldots, N)$, with N_{ai} pixels in azimuth direction and N_{ri} pixels in range direction. The ith phase data segment is shown in Fig. 4. The interferogram is filtered before unwrapping. The data in red rectangle is used to estimate azimuth interferometric fringe frequency. The data in blue rectangle is used to estimate range interferometric fringe frequency.

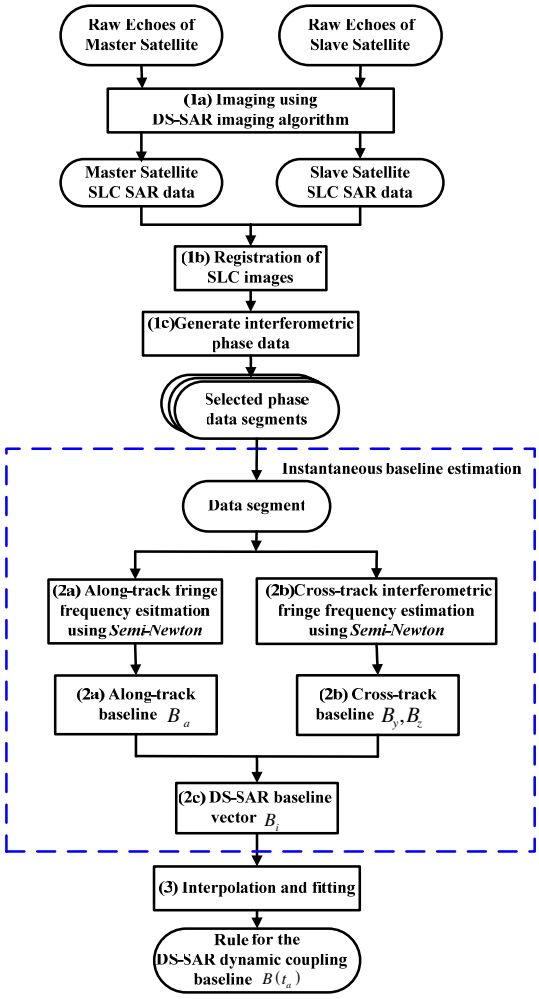

Figure 3. Flowchart of DS-SAR dynamic coupling baseline estimation.

The number of pixels in red rectangle is $N_a^{AT} \times N_r^{AT}$ (the superscript AT represents 'along-track'), with N_a^{AT} data in azimuth direction and N_r^{AT} data in range direction. The phase data are filtered in range direction to reduce phase noise. $N_a^{AT} \times 1$ filtered phase data are used to estimate the azimuth frequency f_{ai} $(i = 1, \ldots, N_a^{AT})$. The average of f_{ai} $(i = 1, \ldots, N_a^{AT})$ will be used as $\Delta f_d(m, s)$ in Equation (16).

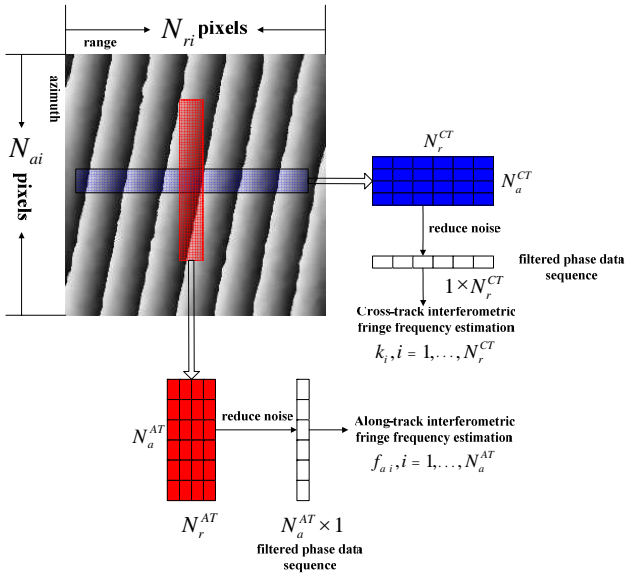

Figure 4. Illustration of 2-D interferometric fringe frequency estimation.

The number of pixels in blue rectangle is $N_a^{CT} \times N_r^{CT}$ (the superscript CT represents 'cross-track'), with N_a^{CT} data in azimuth direction and N_r^{CT} data in range direction. The phase data are filtered in azimuth direction. $1 \times N_r^{CT}$ filtered phase data are used to estimate the cross-track frequency k_i $(i = 1, \ldots, N_r^{CT})$. The estimated frequency k_1, related with the left-most pixel in the blue rectangle, is corresponding to $r_m^{\min}$ in Equation (22). Frequency $k_{N_r^{CT}}$, related with the right-most pixel, is corresponding to $r_m^{\max}$ in Equation (22). Here, $k_{r_m^{\min}} = k_1$ and $k_{r_m^{\max}} = k_{N_r^{CT}}$.

Azimuth frequency and range frequency will be estimated separately. Assume that the filtered phase data sequence is $(p_1, p_2, \ldots, p_L)$ and the ideal frequency sequence relatively is $(f_1, f_2, \ldots, f_L)$. L is the sequence length, which is equal to N_a^{AT} for azimuth frequency estimation and N_r^{CT} for range frequency estimation.

The complex sequence $\left(e^{j\cdot p_{i-M}}, \ldots, e^{j\cdot p_i}, \ldots e^{j\cdot p_{i+M}}\right)$, where $(p_1, p_2, \ldots, p_L)$ are phases, can be modeled as:

$$y_{im} = e^{jmTf_i + j\varphi}, \quad m = -M, \cdots, M \tag{23}$$

It is centralized with the ith data $e^{j\cdot p_i}$. T is the sample interval, φ is the phase noise.

The frequency can be obtained using the maximum likehood estimator of f_i [32],

$$f_i = \begin{cases} \arg\left(\max\limits_f \left|\sum\limits_{m=-M}^{M} y_{im} e^{-jmTf}\right|\right), \varphi \text{ is unkown} \\ \arg\left[\max\limits_f \mathrm{Re}\left(\sum\limits_{m=-M}^{M} y_{im} e^{-jmTf-j\varphi}\right)\right], \varphi \text{ is kown} \end{cases} \tag{24}$$

Based on Equation (24), the frequency can be estimated through two main steps as follows:

1. The coarse frequency estimation$\left(f_1^0, f_2^0, \ldots, f_L^0\right)$, used as the initial value in the iterative method, is obtained through Fourier transform and interpolation.

The frequency of $p_i\,(1 \le i \le L)$ is estimated through the FFT to the finite data sequence $\left(e^{j\cdot p_{i-M}}, \ldots, e^{j\cdot p_i}, \ldots e^{j\cdot p_{i+M}}\right)$ centralized with $e^{j\cdot p_i}$, where $2M+1 < L$. It is assumed that the corresponding data sequence in the frequency domain is $(F_{i-M}, \ldots, F_i, \ldots F_{i+M})$ and the maximum of the sequence$(|F_{i-M}|, \ldots, |F_i|, \ldots |F_{i+M}|)$ is $|F_j|$ $(i-M \le j \le i+M)$. To improve the frequency resolution, the number of data performed Fourier transform must satisfy certain demand [13]. Then the sequence $(F_{j-n}, \ldots, F_j, \ldots, F_{j+n})$ $(n < M)$ can be interpolated to further increase the frequency resolution. The relevant frequency of the maximum of new sequence obtained by interpolation is the coarse estimated frequency f_i^0.

2. Semi-Newton iterative method is employed to improve the frequency estimation precision.

From Equation (24), the instantaneous frequency can be acquired using the maximum likelihood estimator,

$$\max_f \{G(f)\} \tag{25}$$

$$G(f) = \mathrm{Re}\left\{\sum_{m=-M}^{M} y_{im} \cdot e^{-jmTf-j\varphi}\right\} \tag{26}$$

Equation (25) is equivalent to solving the zero point of $G'(f)$, which is the differentiator of $G(f)$. Because φ is unknown, Semi-Newton iterative method is introduced.

$$f_i^{n+1} = f_i^n - \mathrm{Re}\left\{\frac{H'(f_i^n)}{H''(f_i^n)}\right\} \tag{27}$$

$$H(f) = \sum_{m=-N}^{N} y_{im} e^{-jmTf} \tag{28}$$

where n is the iterative time and the coarse estimation f_i^0 in the first step is set to be the initial value in the iterative operation until the demand is satisfied.

5. SIMULATION AND RESULTS

Table 1 shows simulation parameters, where the data-take time is 3 minutes. In this simulation [33–35], ten data segments for even area are selected in along-track direction, and each data segment includes 64 pulses and 1024 range cells.

By modelling the satellite-ground geometry of DS-SAR, SLC images of master and slave satellite SAR are simulated. The simulation results corresponding to the third segment are shown in Fig. 5, where

Table 1. Simulation parameters for DS-SAR system.

Parameter	Value
Satellite height/km	514.000
Satellite velocity/m/s	7600.00
Look angle/deg	30.00
Wavelength/m	0.031
Signal bandwidth/MHz	100.00

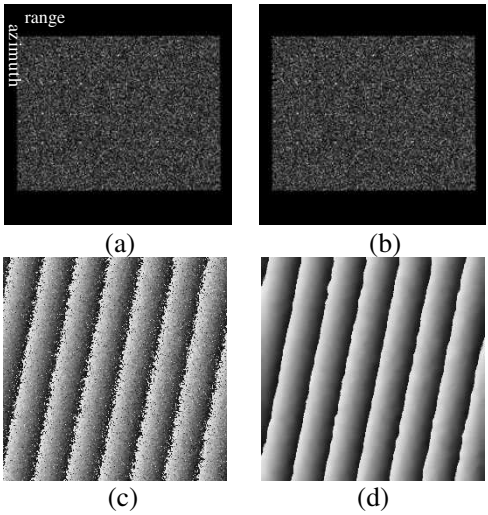

Figure 5. DS-SAR simulation results. (a) master SAR image (SLC), (b) slave SAR image (SLC), (c) interferogram before filtering, (d) interferogram after filtering.

(a) is the image of master satellite SAR and (b) is the image of slave satellite SAR. Fig. 5(c) shows the interferogram given by coarse registration, interpolation, precise registration and interferometric process on both images. To refine the interferogram, phase filtering is performed, and result is shown in Fig. 5(d).

Table 2 shows the estimation results of baseline vector errors of ten segments of interferometric phase data, which include errors of along-track baseline (B_a), errors of horizontal component of cross-track baseline(B_y) and errors of vertical component B_z. From Table 2, precision of along-track baseline estimation achieves millimeter level, while the others achieve centimeter level.

Table 2. Estimation errors of baseline vector/cm.

Phase data No. in azimuth	Error of B_a	Error of B_y	Error of B_z
1	0.34	3.7	−4.2
2	0.27	4.3	8.1
3	−0.81	−0.9	−0.5
4	−0.86	3.0	5.9
5	−0.23	−2.2	4.6
6	0.52	−0.8	1.7
7	−0.19	3.5	−5.1
8	0.83	−6.9	−7.2
9	0.56	2.2	−4.8
10	0.27	4.3	6.7

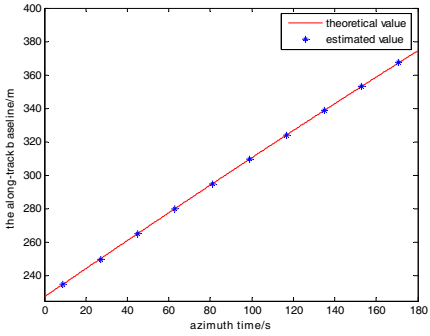

Figure 6. Comparison between estimation and theory value of the along-track baseline (B_a).

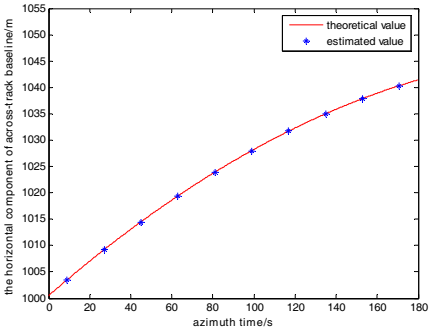

Figure 7. Comparison between estimation and theory value of horizontal component of the cross-track baseline (B_y).

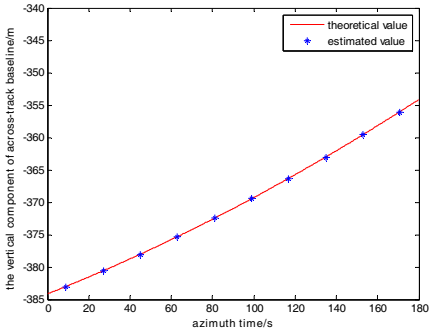

Figure 8. Comparison between estimation and theory value of vertical component of the cross-track baseline (B_z).

Figure 6 is the comparison between estimation and theory value of along-track baseline (B_a). Fig. 7 and Fig. 8 present the comparison results between estimation and theory values of horizontal component B_y and vertical component B_z of cross-track baseline. In all the three figures, the solid line denotes the theory value, while the asterisk is the estimation value. It is shown that estimation values match with theory values well, which validates the proposed approach.

6. CONCLUSION

This paper proposes a novel DS-SAR dynamic and coupling baseline estimation approach based on interferometric phase. Firstly, the mathematical model of interferometric phase is established, and interferometric phase decoupling is proposed. Secondly, the theory of instantaneous baseline estimation is presented, and accurate baseline calculation is deduced considering the earth curvature. Then, the whole framework and detailed implementation of DS-SAR baseline estimation are presented. Furthermore, in order to improve baseline estimation precision, Semi-Newton iterative algorithm is applied to estimate high-precision interferometric fringe frequency. Combining accurate fringe frequency with deduced baseline calculation formula, the baseline estimation achieves centimeter level. Finally, simulation results validate the approach proposed in this paper.

ACKNOWLEDGMENT

The authors would like to thank all the anonymous reviewers for their careful work on this paper. This work was supported in part by the Commission on Science, Technology, and Industry for National Defense of China under Grant No. A2120060006.

REFERENCES

1. Zhou, Y. Q., H. P. Xu, and J. Chen, "Research progress of distributed small satellites synthetic aperture radar," *ACTA Electronic SINICA*, Vol. 31, No. 12, 1939–1944, 2003.
2. Massonnet, D., "Capabilities and limitations of the interferometric cartwheel," *IEEE Trans. Geosci. Remote Sens.*, Vol. 39, No. 3, 506–520, 2001.
3. Wu, B. I., M. C. Yeung, Y. Hara, and J. A. Kong, "InSAR height inversion by using 3-D phase projection with multiple baselines," *Progress In Electromagnetics Research*, Vol. 91, 173–193, 2009.
4. Li, S., H. P. Xu, and L. Q. Zhang, "An advanced Dss-SAR InSAR terrain height estimation approach based on baseline decoupling," *Progress In Electromagnetics Research*, Vol. 119, 207–224, 2011.
5. Liu, D., Y. Du, G. Sun, W.-Z. Yan, and B.-I. Wu, "Analysis of InSAR sensitivity to forest structure based on radar scattering model," *Progress In Electromagnetics Research*, Vol. 84, 149–171, 2008.
6. Ren, K., V. Prinet, and X. Q. Shi, "Comparison of satellite baseline estimation methods for interferometry applications," *IGARSS'03*, Vol. 6, 3821–3823, 2003.
7. Kimura, H. and M. Todo, "Baseline estimation using ground points for interferometric SAR," *IGARSS'97*, Vol. 1, 442–444, 1997.
8. Zhang, X. L., S. J. Huang, and J. G. Wang, "Approaches to estimating terrain height and baseline for interferometric SAR," *Electronics Letters*, Vol. 34, No. 25, 2428–2429, 1998.
9. Chen, J., S. Quegan, and X. Yin, "Calibration of spaceborne linearly polarized low frequency SAR using polarimetric selective radar calibrators," *Progress In Electromagnetics Research*, Vol. 114, 89–111, 2011.
10. Wei, H. J., J. B. Zhu, and D. N. Liang, "An accurate baseline estimate method for rugged terrain utilize rough DEM," *Journal of National University of Defence Technology*, Vol. 32, No. 1, 74–78, 2010.
11. Lin, J. T., J. Hong, and J. W. Hu, "Calibration for spaceborne InSAR baseline vector based on sea surface," *Foreign Electronic Measurement Technology*, Vol. 29, No. 3, 31–34, 2010.
12. Singh, K., N. Stussi, L. K. Kwoh, et al., "Baseline estimation in interferometric SAR," *IGARSS'97*, Vol. 1, 454–456, 1997.
13. Tang, X. Q., M. S. Xiang, and Y. R. Wu. "An improved baseline estimation approach based on the interferometric phases," *Journal*

of Electronics & Information Technology, Vol. 30, No. 12, 2795–2799, 2008.

14. Atwood, D. K., R. M. Guritz, R. R. Muskett, et al, "DEM control in Arctic Alaska with ICESat laser altimetry," *IEEE Trans. Geosci. Remote Sens.*, Vol. 45, No. 11, 3710–3720, 2007.
15. Brown, Jr., C. G., K. Sarabandi, and L. E. Pierce, "Validation of the Shuttle Radar Topography Mission height data," *IEEE Trans. Geosci. Remote Sens.*, Vol. 43, No. 8, 1707–1715, 2005.
16. Ma, L., Z. F. Li, and G. Liao, "System error analysis and calibration methods for multi-channel SAR," *Progress In Electromagnetics Research*, Vol. 112, 309–327, 2011.
17. Dang, Y. W. and W. D. Yu, "Analysis of the along-track baseline decorrelation of distributed small satellites SAR," *Journal of Electronics & Information Technology*, Vol. 29, No. 12, 2863–2866, 2007.
18. Krieger, G., A. Moreira, H. Fiedler, et al., "TanDEM-X: A satellite formation for high-resolution SAR interferometry," *IEEE Trans. Geosci. Remote Sens.*, Vol. 45, No. 11, 3317–3341, 2007.
19. Krieger, G., I. Hajnsek, K. P. Papathanassiou, et al., "Interferometric synthetic aperture radar (SAR) missions employing formation flying," *Proceedings of the IEEE*, Vol. 98, No. 5, 816–843, 2010.
20. Xu, Q., G. S. Liao, and Y. Liu, "3-D baseline error estimation method for distributed small satellites," *Journal of Xidian University*, Vol. 25, No. 4, 668–672, 2008.
21. Liu, Y., Z. M. Wang, and D. Y. Yi, "Associated modeling and error analysis between space states and alimeter baseline of distributed SAR," *Journal of System Simulation*, Vol. 19, No. 15, 3468–3472, 2007.
22. Cumming, I. G. and J. R. Bennett, "Digital processing of SEASAT SAR data," *IEEE International Conference on Acoustics, Speech & Signal Processing*, Vol. 4, 710–718, 1979.
23. Huang, Y., *Research on Image Formation Technology for High Resolution SAR*, Beihang University, Beijing, 1999.
24. Sun, J., S. Mao, G. Wang, and W. Hong, "Polar format algorithm for spotlight bistatic SAR with arbitrary geometry configuration," *Progress In Electromagnetics Research*, Vol. 103, 323–338, 2010.
25. Xu, H. P., Y. Q. Zhou, and C. S. Li, "Signal model of single look complex image for distributed small satellite synthetic aperture radar," *Journal of Electronics & Information Technology*, Vol. 26, 168–172, 2004.

26. Guo, D., H. Xu, and J. Li, "Extended wavenumber domain algorithm for highly squinted sliding spotlight SAR data processing," *Progress In Electromagnetics Research*, Vol. 114, 17–32, 2011.
27. Xu, W., P. Huang, and Y.-K. Deng, "Multi-channel Spcmb-Tops SAR for high-resolution wide-swath imaging," *Progress In Electromagnetics Research*, Vol. 116, 533–551, 2011.
28. Liu, Q., W. Hong, W. Tan, Y. Lin, Y. Wang, and Y. Wu, "An improved polar format algorithm with performance analysis for geosynchronous circular SAR 2D imaging," *Progress In Electromagnetics Research*, Vol. 119, 155–170, 2011.
29. Sansosti, E., P. Berardino, M. Manunta, et al., "Geometrical SAR image registration," *IEEE Trans. Geosci. Remote Sens.*, Vol. 44, No. 10, 2861–2870, 2006.
30. Nitti, D. O., R. F. Hanssen, A. Refice, et al, "Impact of DEM-assisted coregistration on high-resolution SAR interferometry," *IEEE Trans. Geosci. Remote Sens.*, Vol. 49, No. 3, 1127–1143, 2011.
31. Li, C. and D. Y. Zhu, "A residue-pairing algorithm for InSAR phase unwrapping," *Progress In Electromagnetics Research*, Vol. 95, 341–354, 2009.
32. Abatzoglou, T. J., "A fast maximum likelihood algorithm for frequency estimation of a sinusoid based on Newton's method," *IEEE Trans. on Acoustics, Speech and Signal Processing*, Vol. 33, No. 1, 77–89, 1985.
33. Xu, H. P., J. Chen, B. F. Wang and Y. Q. Zhou, "Quick method of distributed small satellite synthetic aperture radar single-look complex image simulation," *Journal of Beijing University of Aeronautics and Astronautics*, Vol. 32, No. 4, 445–449, 2006.
34. Chang, Y.-L., C.-Y. Chiang, and K.-S. Chen, "SAR image simulation with application to target recognition," *Progress In Electromagnetics Research*, Vol. 119, 35–57, 2011.
35. Zhang, M., Y. W. Zhao, H. Chen, and W.-Q. Jiang, "SAR imaging simulation for composite model of ship on dynamic ocean scene," *Progress In Electromagnetics Research*, Vol. 113, 395–412, 2011.